Journal of Statistical Physics, Vol. 42, Nos. 3/4, 1986

The Pressure of a Hard Sphere Fluid on a Curved Surface

M. F. Wehner[1,2] and W. G. Wolfer[1]

Received October 9, 1984; revised April 1, 1985

Utilizing the integral equation approach to the hard sphere fluid system developed in the preceding paper, the hard sphere–hard wall interaction is studied. For the case of a flat wall, perturbation solutions of the integral equation valid to second and third order in the packing fraction, y, are derived. For a surface of arbitrary curvature, an equation of state valid to second order in the packing fraction is also derived. When applied to very small cavities, it is found that the pressure at high densities is significantly higher than it would be for a flat wall.

KEY WORDS: Hard sphere fluid; wall-atom distribution function; wall contact values; equation of state.

1. INTRODUCTION

In the preceding article,[1] hereafter referred to as I, we have presented a new nonlinear integral equation describing the radial distribution function of a hard sphere fluid system. For a test particle of arbitrary radius, R, surrounded by particles of a common radius, a, the radial distribution function, $g_R(x)$ satisfies the integral equation,

$$\ln g_R(x) = -y g_a(a) \frac{6}{a} \int_{\infty}^{x} dx' \int_{\tilde{x}_0}^{\tilde{x}_1} g_R(\tilde{x})\, f(x', \tilde{x})\, d\tilde{x} \tag{1}$$

where

$$f(x', \tilde{x}) = \frac{[(x' \pm R)^2 - (\tilde{x} \pm R)^2 + 4a^2](\tilde{x} \pm R)}{8a^2(x' \pm R)^2} \tag{2}$$

[1] Fusion Technology Institute, 1500 Johnson Drive, University of Wisconsin–Madison, Madison, Wisconsin 53706.

[2] Current address: Lawrence Livermore National Laboratory, Livermore, California 94550.

0022-4715/86/0200-0509$05.00/0

and

$$\tilde{x}_0 = x' - 2a, \qquad \tilde{x}_1 = x' + 2a \qquad \text{for} \quad 3a \leqslant x' < 5a$$

or

$$\tilde{x}_0 = a, \qquad \tilde{x}_1 = x' + 2a \qquad \text{for} \quad a \leqslant x' \leqslant 3a$$

In this paper, we will apply the perturbation solution obtained in I by extending Shinomoto's method[2] to cases where the radius of the test particle is different from the radii of the generic particles.

In Section 2, we will perform the limit $R \to \infty$ to find the hard sphere–hard wall distribution functions in both the second- and third-order approximations.

In Section 3, we will evaluate the radial distribution function to second order at $x = a$ for a general choice of R to find an equation of state for a dense fluid in a very small cavity.

2. THE WALL–ATOM DISTRIBUTION FUNCTION

The probability of finding a hard sphere atom a certain distance away from a hard wall is simply found by performing the limit $R \to \infty$ and proceeding in the same fashion as in the calculation of the pair distribution function in I. This probability can be interpreted as the density profile near the wall.

The development then picks up at Eq. (27) of I. Performing the limit $R \to \infty$ yields

$$\lim_{R \to \infty} f(x, \tilde{x}) = \frac{x - \tilde{x}}{4a^2} \quad \text{and} \quad \lim_{R \to \infty} \psi_1(\tilde{x}) = \frac{(\tilde{x}) - 3a)^2 (x + 3a)}{4a^3}$$

The second-order potential evaluated at $R \to \infty$ becomes

$$\frac{\phi_2^{\mathrm{I}}(x, y, R = \infty)}{yKT} = \left(1 + \frac{5}{2} y\right)\left[-\frac{(x - 3a)^2 (x + 3a)}{4a^3}\right] + \frac{y}{20a^2}[45x^2 - 138ax - 67a^2] \tag{2a}$$

$$= -[\psi_2^{\mathrm{Ia}}(x, R = \infty) + y\psi_2^{\mathrm{Ib}}(x, R = \infty)] \tag{2b}$$

for the region $a \leqslant x \leqslant 3a$ and

$$\frac{\phi_2^{\mathrm{II}}(x, y, R = \infty)}{y^2 KT} = \frac{(x - 5a)^4 (x^2 + 14ax + 25a^2)}{320a^6} \tag{3a}$$

$$= -\psi_2^{\mathrm{II}}(x, R = \infty) \tag{3b}$$

for $3a \leqslant x \leqslant 5a$. Here, y is the packing fraction defined as

$$y = \frac{4\pi}{3} a^3 n$$

The second-order hard sphere–hard wall distribution function is therefore given as

$$g_{\infty}^2(x) = \begin{cases} 0, & a \geqslant x \\ \exp[y\psi_2^{\mathrm{Ia}}(x) + y^2\psi_2^{\mathrm{Ib}}(x)], & a \leqslant x \leqslant 3a \\ \exp[y^2\psi_2^{\mathrm{II}}(x)], & 3a \leqslant x \leqslant 5a \\ 1, & x \geqslant 5a \end{cases} \tag{4}$$

Figure 1 shows this distribution function as a function of x/d, where x is the distance from the center of the atom to the surface of the wall and d is the diameter of the atom. Again, as for the second-order pair distribution function, the characteristic oscillatory behavior is absent in the second-order perturbation.

To find the third-order solution, it is necessary to evaluate the integrals of Eqs. (34) to (36) in I. Since the functions in Eq. (2) and (3) are

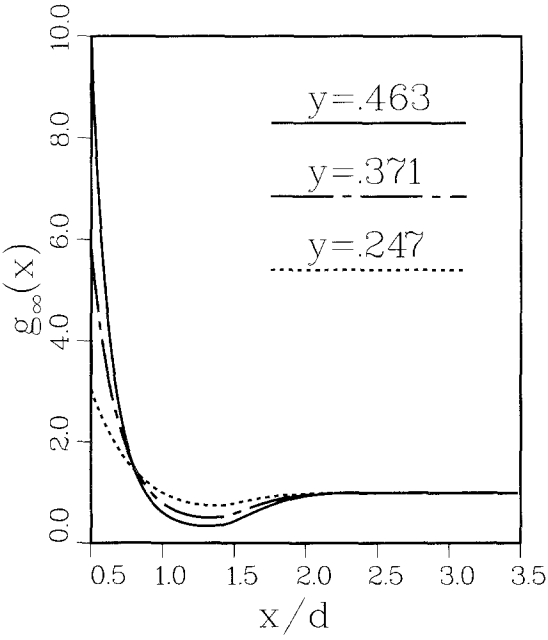

Fig. 1. Second-order perturbation solution of Eq. (1) in the limit $R \to \infty$ evaluated at various packing fractions.

simple polynomials, these integrations are elementary. The third-order radial distribution is given as

$$g_R^3(x) = \begin{cases} 0, & a > x \\ \exp[y\psi_3^{\mathrm{Ia}}(x) + y^2\psi_3^{\mathrm{Ib}}(x) + y^3\psi_3^{\mathrm{Ic}}(x)], & a \leqslant x \leqslant 3a \\ \exp[y^2\psi_3^{\mathrm{IIa}}(x) + y^3\psi_3^{\mathrm{IIb}}(x)], & 3a \leqslant x \leqslant 5a \\ \exp[y^3\psi_3^{\mathrm{III}}(x)], & 5a \leqslant x \leqslant 7a \\ 1, & x \geqslant 7a \end{cases} \tag{5}$$

Noting that the second-order pair distribution function at the contact distance is

$$g_a^2(a) = 1 + \frac{5}{2}y + \frac{1009}{280}y^2 \tag{6}$$

the relationships defining the third-order hard wall–hard atom distribution function become

$$\psi_3^{\mathrm{Ia}}(x) = \psi_2^{\mathrm{Ia}}(x) \tag{7}$$

$$\psi_2^{\mathrm{Ib}}(x) = \psi_2^{\mathrm{Ib}}(x)$$

$$\psi_3^{\mathrm{IIa}}(x) = \psi_2^{\mathrm{II}}(x)$$

$$\psi_3^{\mathrm{Ic}}(x) = \frac{1009}{280}\psi_3^{\mathrm{Ia}}(x) + \frac{5}{2}\psi_3^{\mathrm{Ib}}(x) + \left(- \frac{x^9 + 9x^8a + 396a^7a^2 - 4284x^6a^3}{107520a^9} + \frac{-1134x^5a^4 + 200718x^4a^5 - 1177092x^3a^6 + 3291444x^2a^7}{107520a^9} + \frac{-5116185xa^8 + 2662769a^9}{107520a^9} \right)$$

$$\psi_3^{\mathrm{IIb}}(x) = \frac{5}{2}\psi_3^{\mathrm{IIa}}(x) + \left(\frac{5x^9 - 45x^8a - 828x^7a^2 + 14448x^6a^3 - 64386x^5a^4}{53760a^9} + \frac{-83034x^4a^5 + 1188516x^3a^6 - 750888x^2a^7}{53760a^9} + \frac{-8917277xa^8 + 14726719a^9}{53760a^9} \right)$$

and

$$\psi_3^{\mathrm{III}}(x) = \left(\frac{-x^9 + 9x^8a + 396x^7a^2 - 6972x^6a^3 + 14994x^5a^4 + 450702x^4a^5}{107520a^9} + \frac{-4004868x^3a^6 + 11495988x^2a^7 - 1058841xa^8 - 33765263a^9}{107520a^9} \right)$$

This distribution function, $g^3_\infty(x)$, is plotted in Fig. 2 as a function of x/d for various packing functions, y. As was true for the pair distribution, oscillations appear in the third-order solution. However, at high densities, the value of the distribution function at the contact point is significantly lowered in passing from the second to third order perturbation solution. In Figs. 3 and 4, comparisons between the Monte Carlo results of Snook and Henderson[3] and the second- and third-order perturbation solutions are shown graphically for two different packing fractions. At the lower density, Fig. 3, the third-order solution agrees fairly well for $x/d < 1$. However, the height and location of the peak is not predicted very accurately. At the higher density, the disagreement is, of course, more pronounced. However, a closer inspection of both figures reveals that the higher second-order contact values are closer to reality. This accounts for the excellent agreement Shinomoto found between the second-order equation of state (for a flat wall) and the more conventionally derived equations of state. This does not mean that the third-order results are incorrect but rather illustrates the slow convergence of the solution of the integral equation (1) with a perturbation method. In Fig. 5, a comparison between the solution of the Per-

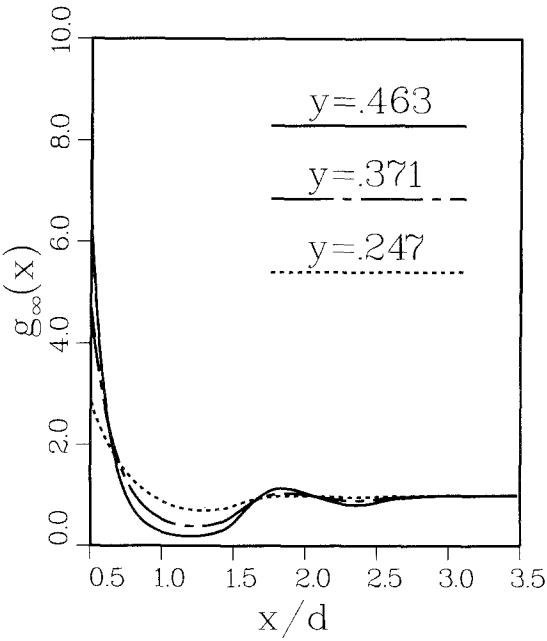

Fig. 2. Third-order perturbation solution of Eq. (1) in the limit $R \to \infty$ evaluated at various packing fractions.

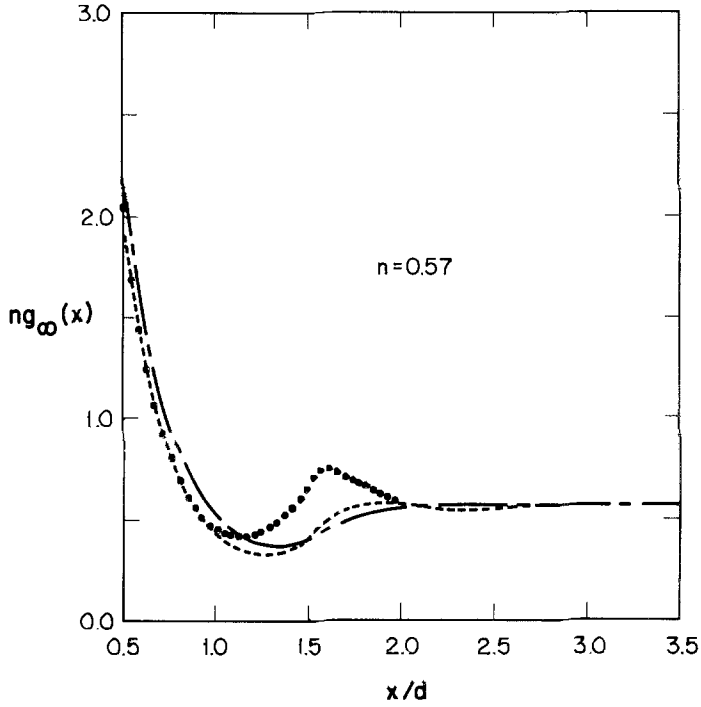

Fig. 3. Comparison between the Monte Carlo results of Snook and Henderson and the second- and third-order perturbation solutions of Eq. (1) at the bulk density $n = 0.57$ (corresponding to $y = 0.298$). The Monte Carlo results are indicated by the filled circles. The chain dash line represents the second-order perturbation. The dashed line represents the third-order perturbation.

cus–Yevick equation[4] for the hard wall–hard sphere system and the perturbation solutions is made at the relatively high packing fraction $y = 0.419$. Again at this high density, the number of oscillations is greater than the third-order perturbation solution allows, hence the agreement is rather poor.

3. EQUATION OF STATE FOR HARD, CURVES SURFACES

The success of the second-order perturbation solution in predicting the contact value of the radial distribution for a flat wall suggests that the second-order approximation may be useful for finding accurate contact values for curved surfaces. For an arbitrary value of the test particle's curvature, R, the integrands involved in Eqs. (34)–(36) of I become quite complicated rational functions. Therefore, in order to avoid errors, the

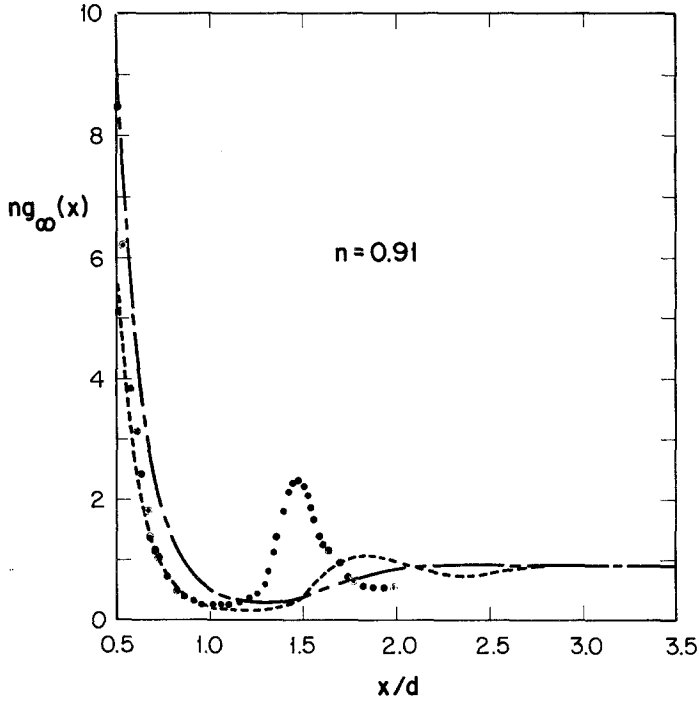

Fig. 4. Same as Fig. 3 except for the higher bulk density $n = 0.91$ (corresponding to $y = 0.476$).

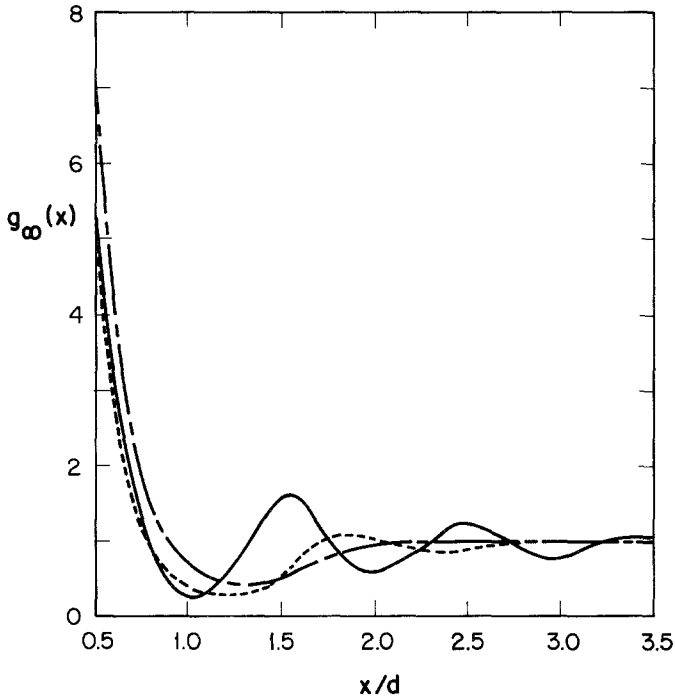

Fig. 5. Comparison between the solution of the Percus–Yevick equation for the hard sphere–hard wall system and the second- and third-order perturbation solutions of Eq. (1) for the bulk density $n = 0.8$ (corresponding to $y = 0.419$). The perturbation solutions are indicated in the same way as they are in Figs. 3 and 4. The solid lines represent the PY solution.

integrations have been done in closed form with the algebraic manipulation routine REDUCE2.[5]

The result for the second-order potential evaluated at $x = a$ is given as

$$\phi_2^1(x = a,\ y,\ R)/kT = M(a, y,\ R)/N(a,\ y,\ R) \tag{8}$$

where

$$\begin{aligned} M(a,\ y,\ R) &= 478953a^9y - 459270a^9 + 358668a^8Ry - 3061800a^8R \\ &\quad - 959364a^7R^2y - 6327720a^7R^2 - 1864296a^6R^3y - 6667920a^6R^3 \\ &\quad - 1491210a^5R^4y - 4207140a^5R^4 - 683424a^4R^5y - 1693440a^4R^5 \\ &\quad - 193284a^3R^6y - 441000a^3R^6 - 33528a^2R^7y - 72240a^2R^7 \\ &\quad - 3287aR^8y - 6790aR^8 - 140R^9y - 280R^9 \end{aligned} \tag{9}$$

and

$$\begin{aligned} N(a,\ y,\ R)/70 &= 6561a^9 + 24057a^8R + 37908a^7R^2 + 34020a^6R^3 \\ &\quad + 19278a^5R^4 + 7182a^4R^5 + 1764a^3R^6 + 276a^2R^7 \\ &\quad + 25aR^8 + R^9 \end{aligned} \tag{10}$$

The equation of state in the second-order approximation is then given by the contact value

$$z(y,\ R) = p/nkT = g_R^2(a) = \exp[-\phi_2^1(a,\ y,\ R)/kT] \tag{11}$$

For $R = \pm\infty$, this reduces to Shinomoto's result for the flat wall[2]

$$\begin{aligned} z(y,\ \infty) &= \exp\left[4y\left(1 + \frac{y}{2}\right)\right] \simeq 1 + 4y + 10y^2 + 18.67y^3 + 28.67y^4 \\ &\quad + 37.87y^5 + \cdots \end{aligned} \tag{12}$$

As Shinomoto has pointed out, this compares very favorably with the Ree and Hoover virial expansion.[6] In Fig. 6a, the ratio of the gas pressure on a curved surface to the pressure on a flat surface as a function of the hard sphere packing fraction is plotted for various different positive radii to show the relative effect of curvature. Note that the compressibility factor and hence the pressure decreases with decreasing radius of curvature for a given packing fraction. As a result, the gas-kinetic pressure on a protrusion in a flat wall is actually less than the pressure on the flat portions.

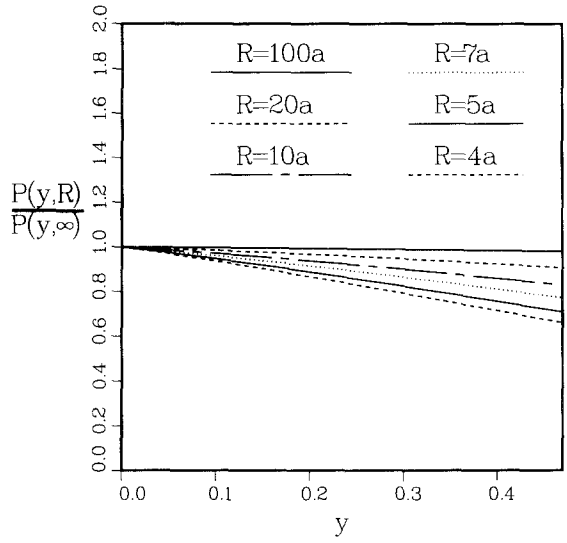

(a)

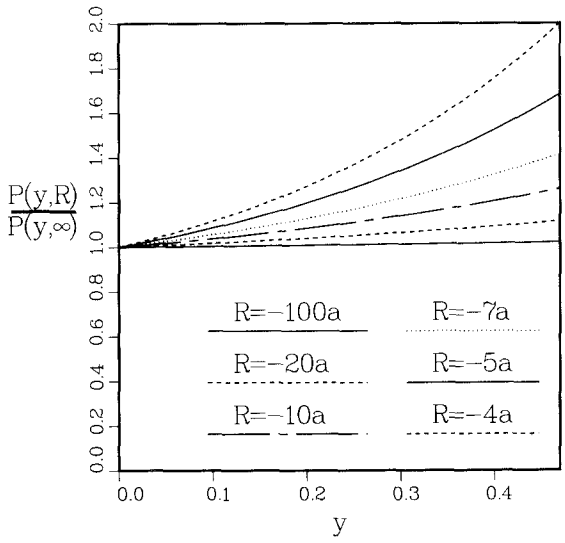

(b)

Fig. 6. (a) Ratio of pressures on a convex and a flat surface vs. packing fraction. Radii of curvature given in units of the gas atom radius. (b) Ratio of pressures on a concave or cavity surface and a flat surface vs. packing fraction. The cavity radii R are in units of the gas atom radius.

For the case of small cavities the situation reverses. The curvature is now concave and characterized by negative values of R in the present convention. As the results in Fig. 6b show the compressibility factor and hence the pressure increases as the radius of curvature becomes smaller in absolute terms. Hence, for the same packing fraction, a gas exerts a greater gas-kinetic pressure on a small cavity than on a larger one. This can be simply explained by the observation that gas atoms impinging on a concave surface will on average impart a greater component of linear momentum perpendicular to this surface than when the surface is flat, or worse yet, convex in curvature. This observation also makes it plausible that a curvature effect will only become significant when the curvature radius approaches the atomic radius of the gas particles. Such systems of small cavities can often occur in the defects of an irradiated metal which has been subject to a supersaturation of light atoms such as helium or hydrogen.[10]

A direct quantitative comparison of Eq. (11) with the Percus–Yevick theory is available for positive R. Lebowitz *et al.*[8] has shown that the PY contact values obtained from the compressibility relation are given for a mixture of hard spheres by

$$g_{R_i}(R_j) = (1-\xi_3)^{-1} + \frac{6\xi_2}{(1-\xi_3)^2}\left(\frac{R_i R_j}{R_i + R_j}\right) + \frac{12\xi_2^2}{(1-\xi_3)^3}\left(\frac{R_i R_j}{R_i + R_j}\right)^2 \tag{13}$$

where

$$\xi_l = \frac{\pi}{6}\sum_{l=1}^{m} \rho_i (2R_i)^l \tag{14}$$

and m is the number of different species.

To compare the present results with the PY theory, the limiting case of a binary mixture with one component's density approaching zero is assumed. If $R_1 = a$, $R_2 = R$, $\rho_1 = n$, and $\rho_2 \to 0$, then the moments of Eq. (14) become

$$\begin{aligned} \xi_3 &= y \\ \xi_2 &= y/2a \end{aligned} \tag{15}$$

As the PY theory is not exact, a different expression for the contact values can be derived using the virial theorem. The virial contact values are related to the compressibility contact values by

$$g_{R_i}^V(R_j) = g_{R_i}^C(R_j) - \frac{12\xi_3\xi_2^2}{(1-\xi_3)^3}\left(\frac{R_i R_j}{R_i + R_j}\right)^2 \tag{16}$$

In Fig. 7a, the results of Eqs. (9)–(11) are plotted along with those obtained from the compressibility and virial expressions of the PY theory for $R = 100a$. As this radius of curvature represents a very nearly flat sur-

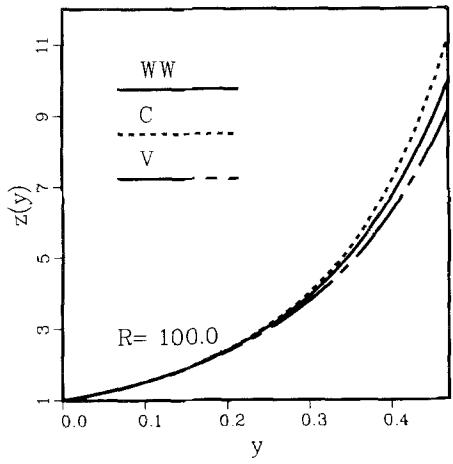

(a)

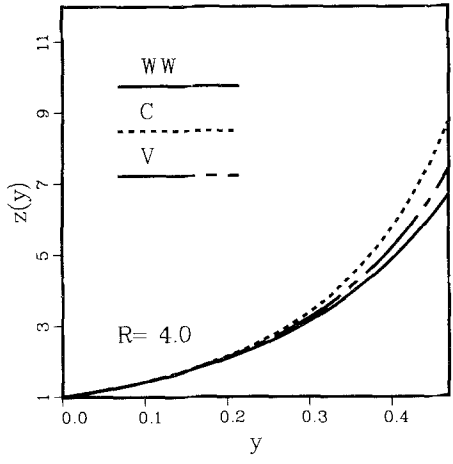

(b)

Fig. 7. (a) Compressibility factors vs. hard sphere packing fraction for a convex surface with a radii of curvature 100 times the radius of the impinging hard spheres. Solid line, present results; dashed line, PY compressibility prediction; chained dash line, PY virial prediction. (b) Same as Fig. 7(a) but for $R = 4a$.

face, the present results lie between the two different PY predictions consistent with Shinomoto's original paper. However, as the radius of curvature is decreased, the difference between the PY compressibility and virial curves begins to shrink. Although this difference never vanishes, at a certain value of R, the contact values predicted by Eqs. (9)–(11) will lie outside of the two PY curves. This is seen for a value of $R = 4a$ as shown in Fig. 7b. At $R \sim 10a$, the virial contact values and the present results coincide.

5. CONCLUSIONS

Analytic expressions are derived in the flat wall limit for the second- and third-order perturbation solutions of a new integral equation for the hard sphere fluid system. As a systematic result of the perturbation method, the characteristic oscillations of the radial distribution function are not observed until the third-order approximation. Even though the perturbation solution converges rather slowly for large average densities when judged by the wall distribution function, the gas-kinetic pressure obtained on a flat surface with the second-order perturbation solution is already in excellent agreement with the Carnahan–Starling equation for a hard-sphere gas.[7]

When evaluating the pressure on a curved surface, the situation is not quite so clear. For very small radii of curvature, the second-order perturbation solution slightly overpredicts the difference between the flat wall and curved wall pressures when compared to the Percus–Yevick theory. This discrepancy is more than likely a result of the relative low order of the solution in the packing fraction. However, the intuitive ideas introduced by Shinomoto provide an elementary understanding of why the gas kinetic pressure exerted in a very small cavity in a solid is significantly larger than the pressure exerted on a flat wall: the pressure represents the average momentum transfer to the wall by impacting spheres. Contained in this average is an average over the cosine of the impact direction. For a small cavity, more of the impacts of the hard spheres with the wall are nearly perpendicular than in the case of a flat wall or even a convex wall. As a result, the angular average is larger, and the pressure increases with decreasing cavity radius. This geometrical interpretation of the pressure enhancement on a curved surface also forms one of the central ideas of the scaled particle theory for liquids.[9]

ACKNOWLEDGMENT

This research was supported by the U.S. Department of Energy under contract DE-AC02-82ER52082 with the University of Wisconsin.

REFERENCES

1. M. F. Wehner and W. G. Wolfer, *J. Stat. Phys.* **42**:493 (1986).
2. S. Shinomoto, *Phys. Lett.* **89A**:19 (1982).
3. I. K. Snook and D. Henderson, *J. Chem. Phys.* **68**:2134 (1978).
4. D. Henderson, F. F. Abraham, and J. A. Barker, *Mol. Phys.* **31**:1291 (1976).
5. A. C. Hearn, "REDUCE2 User's Manual," 2nd ed.,University of Utah, UCP-19, March 1973.
6. F. H. Ree and W. G. Hoover, *J. Chem. Phys.* **40**:939 (1964).
7. N. F. Carnahan and K. E. Starling, *J. Chem. Phys.* **51**:635 (1969).
8. J. L. Lebowitz, *Phys. Rev.* **133**:A895 (1964); and J. L. Lebowitz, E. Helfand, and E. Praestgaard, *J. Chem. Phys.* **43**:774 (1965).
9. H. Reiss, *Adv. Chem. Phys.* **9**:1 (1967).
10. W. G. Wolfer and F. A. Garner, *Radiation Effects* **78**:801 (1983).